Applied Energy 165 (2016) 748–758

Contents lists available at ScienceDirect

Applied Energy

journal homepage: www.elsevier.com/locate/apenergy

A signal-based method for fast PEMFC diagnosis

E. Pahon [a,*], N. Yousfi Steiner [a,b], S. Jemei [a], D. Hissel [a], P. Moçoteguy [c]

[a] FEMTO-ST UMR CNRS 6174, FCLAB Research Federation FR CNRS 3539, University Bourgogne Franche-Comte, rue Ernest Thierry Mieg, 90010 Belfort Cedex, France
[b] LABEX ACTION CNRS, FEMTO-ST UMR CNRS 6174, FCLAB Research Federation FR CNRS 3539, University Bourgogne Franche-Comte, rue Ernest Thierry Mieg, 90010 Belfort Cedex, France
[c] EIFER, European Institute for Energy Research, Emmy-Nother Strasse 11, Karlsruhe, Germany

HIGHLIGHTS

- A novel signal-based approach is proposed for the PEMFC fault diagnosis.
- The state-of-health is estimated by using the wavelet transform approach.
- The results are coming from the analysis of the energy and the entropy of a signal.
- The robustness of the method is carried out by using a large database.
- Experimental data verify the efficiency of the method for an air supplying fault.

ARTICLE INFO

Article history:
Received 14 September 2015
Received in revised form 27 November 2015
Accepted 17 December 2015
Available online 8 January 2016

Keywords:
Proton exchange membrane fuel cell
Fault diagnosis
Wavelet transform

ABSTRACT

This paper deals with a novel signal-based method for fault diagnosis of a proton exchange membrane fuel cell (PEMFC). Thanks to an in-lab test bench used for the experimental tests, various parameters can be recorded as electrical or fluidic measurements. The chosen input signal for the diagnosis uses no additional expensive and no intrusive sensors specifically dedicated for the diagnosis task. It uses insofar only the already existing sensors on the system. This paper focuses on the detection and identification of a high air stoichiometry (HAS) fault. The wavelet transform (WT) and more precisely the energy contained in each detail of the wavelet decomposition is used to diagnose quickly an oversupply of air to the fuel cell system. Finally, some experimental results are presented according to different input signals, in order to prove the efficiency of the patented method.

1. Introduction

The main challenges for the fuel cell system are to reduce its cost, to improve its reliability and to extend its lifetime. The department of energy (DoE) sets some objectives to be met by the end of 2015, both for automotive and stationary applications [1]. These objectives mainly concern the cost and the lifetime. The cost of fuel cell power systems must be reduced before they can be competitive with gasoline internal combustion engines (ICEs). In fact, conventional automotive ICE power plants currently cost about US$25–US$35/kW (August 2011); thus, a fuel cell system needs to cost less than US$30/kW [2,3] to be competitive. A significant fraction of the cost of a PEM fuel cell comes from precious-metal catalysts that are currently used on the anode and cathode for the electrochemical reactions. In addition, fuel cell power systems will be required to be as durable and reliable as current automotive engines (i.e., 5000 h lifespan [150,000 miles equivalent] with less than 10% loss of performance by the end of life) and able to function over the full range of external environmental conditions (−40°C to +40°C) [4]. The current fuel cell lifetime remains still too low (about 2500 h for a PEMFC under actual automotive constraints, which is the main technology used for cars) [5]. Some technical and technological solutions to improve the performances of fuel cells exist. Diagnosis methods can also be associated to prevent abnormal or non-optimal operating conditions for the fuel cell system, in order to improve the fuel cell reliability. A review resumes the main factors affecting the lifetime of PEMFC in vehicle applications [6]. The authors analyze the reasons of the degradation of fuel cell and present some mitigation measures during the fuel cell operation. Based on the lifetime problem, diagnosis researches and approaches aim to find solutions to improve the fuel cell lifespan. Various kinds of fault diagnosis exist and can be classified in two main approaches: the model-based

* Corresponding author. Tel.: +33 384 583 628; fax: +33 384583636.
E-mail addresses: elodie.pahon@univ-fcomte.fr (E. Pahon), nadia.steiner@univ-fcomte.fr (N. Yousfi Steiner), samir.jemei@univ-fcomte.fr (S. Jemei), daniel.hissel@univ-fcomte.fr (D. Hissel), philippe.mocoteguy@eifer.org (P. Moçoteguy).

http://dx.doi.org/10.1016/j.apenergy.2015.12.084
0306-2619/

approaches [7] and the non model-based [8] approaches. The first ones takes into account the physical behavior of the fuel cell system in order to build a valid model of the fuel cell. This model is performed to generate residuals that are used for the diagnosis task. In [9] an in [10], the authors present stack models to analyze parametric study of the stack only. In [9] a one-dimensional model is developed. In [11], it is a zero-dimensional and steady-state PEMFC model which is proposed. The development comprises various types of heat exchangers, compressors, pumps, separators. The aim is to study the thermal and water management of a PEMFC in fork-lift-truck power system. Thus, a semi-empirical solution is used to reproduce the experimental polarization curves of the fuel cell. In [12], a quantitative model-based fault detection and diagnosis approach for building applications that employs a state observer and dynamic model-based is proposed. This approach is developed in order to detect and diagnose some faults which occur on heating, ventilation and air conditioning systems. In [13] a fuel cell stack model is realized thanks to Aspects Dynamics™ simulation tool to study the effect of nitrogen crossover on purging strategy in PEM fuel cell systems. In [14], a model of a 5-kW PEM fuel cell system is developped based on previous works [15]. The model is composed of four elements: a compressor that supplies air, the fuel cell stack, a pressure control valve that drives the pressure inside the cathode chamber and a humidifier. The authors focus on the air group control problem. The entire fuel cell system is modeled in details in order to observe the evolution of internal state variables during a power delivery operation. The non-model based approaches do not require any knowledge of the whole internal behavior of this multiphysics system. The principle is based on signals or datas acquired during experimental tests which are used to teach the diagnosis algorithm in order to recognize, later, the same state of health (SoH) as learned. The methodology presented in this paper belongs to the second category: it is a signal-based approach that uses a mathematical transformation called wavelet transform (WT). The Fourier transform [16] is used to reveal the frequency content of a signal $s(t)$ but it does not allow to localize in time some events such as pulses, jumps and frequency variations which can appear in the signal [17,18]. The WT belongs to the multi-resolution analysis methods class. This approach allows showing some local features under different scales and time localizations of a signal [19]. The WT is used in different contexts of research as wind speed prediction [20,21] or for price forecasting [22], also for the fault diagnosis for temperature, flow rate and pressure sensors in variable air volume systems and for the energy management of an fuel cell hybrid vehicles [23]. In this paper, the aim is to generalize a signal-based fault diagnosis method to several types of fuel cells. Previously, a method is patented on a SOFC system which operate in different operating conditions. By analyzing the energy and the entropy behaviors, the state of health of the SOFC is determined. Based on this efficient results and on the good performance of the signal-based approach for fault diagnosis, the methodology is transposed to the PEMFC system. A specific fault is studied in this paper: a high air stoichiometry fault. The stoichiometry is an important parameter on a PEMFC system. So, the aim is to diagnose the fuel cell SoH as fast as possible by reproducing the same approach tested in the patent [24] on the SOFC system. In this way, the same specifications are used and tested on a PEMFC system. Experimental tests are performed on a 40-cell stack, in different stoichiometry ratios, in order to obtain a large database available for the signal-based method. Like in the patent [24], the estimation of the SoH is based on voltage signals coming from sensors available on the fuel cell test bench. It can be notice that the signal-based approach is well adapted to the fuel cell voltage signals [25]. This paper is organized as follows: firstly, the test bench and the fuel cell used to achieve experimental testing are presented. The protocols for testing the normal and the abnormal operating conditions will be described in the Section 2.2. Thereafter, the novel and patented signal-based fault diagnosis method based on WT is explained. The wavelet decomposition steps and the focus on the energy contained in the inlet signal are presented in the following section. Finally, some diagnosis results based on three different input signals are given in Section 4.

2. Experimental setup

2.1. Experimental equipments

The experimental tests are performed on an electrochemical 40-cell stack assembly (Fig. 1). The experiments have been completed in the frame of a national French ANR project called DIAPASON 2 [26], which focuses on the diagnosis of PEMFC by using non-intrusive methods. The final aim of this project ended in 2013 was to realize an embedded system capable of diagnosing fuel cell system on-line. Algorithms were implemented in order to make real-time diagnosis by taking into account an abnormal increase of the fuel cell temperature, an electrical power converter short circuit problem, a low air supply and so on [27–29]. Some specifications about the considered PEMFC stack are given in Table 1.

The 40-cell stack is tested on a test bench which is designed for testing up to 10 kW PEM fuel cell stacks. The considered test bench is presented on Fig. 2. Various measurements can be obtained in order to detect a deviation from the nominal operating conditions. Over time, a list of standard parameters measured was defined. It includes electrical basic measurements (stack and cell voltages, load current and electrical power) and fluidic parameters as pressure, mass flow, humidity and temperature.

From left to right on Fig. 2, there are the air and the hydrogen supplies with mass flow controllers. Then, two bubblers are available to humidify the inlet gases. The humidity can be adjusted by changing the bubbling type humidifier temperature. The temperature is maintained thanks to heating pipes rolled up around gas inlets. A cooling circuit is designed to refresh the fuel cell in order to control the stack temperature at a given value. When a heating problem appears, some iced-water is injected into the primary deionised water circuit through an exchange device. For each gas input and output, the pressure, the humidity and the temperature sensors provide full operating conditions. The stack voltage, the cell voltages and the load current are recorded too. All acquired

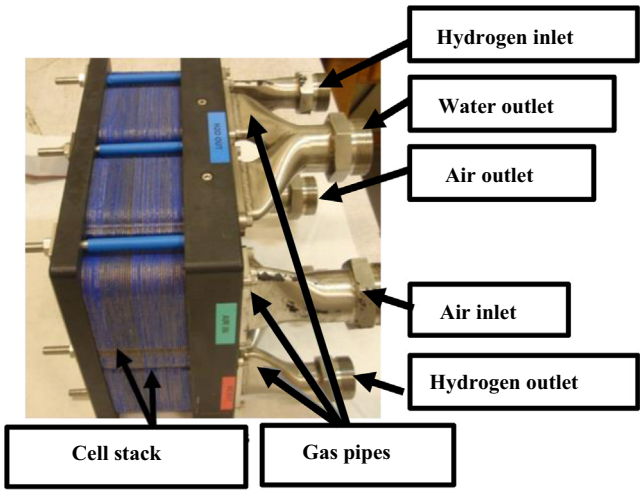

Fig. 1. 40-cell stack with specified inputs and outputs.

Table 1
40-cell stack specifications (nominal operating conditions).

Parameter	Value
Number of cells	40
Hydrogen stoichiometry	1.5
Air stoichiometry	2
Air inlet pressure	150 kPa
Hydrogen inlet pressure	150 kPa
Differential of anode and cathode pressures	30 kPa
Stack temperature (at the output of the cooling circuit)	80 °C
Anode relative humidity	50%
Cathode relative humidity	50%
Nominal flow of the cooling circuit	9.8 l/min
Active area	220 cm^2
Current density	0.5 A/cm^2
Initial average voltage per cell	0.7 V 0.5 A/cm^2
Nominal electrical power	3080 W

parameters are stored and displayed on a dedicated Labview interface thanks to National Instrument devices.

2.2. Experimental protocols

The manufacturer supplied the protocols to start and stop the fuel cell system. Some important steps have to be followed up to avoid damages on the fuel cell stack. Some rules about the temperature and the pressure have to be respected. The last stage is to wait for the good humidity by ordering an air dew point temperature setpoint. When the given temperature is reached, the fuel cell could be placed in the nominal operating conditions, given in Table 1. From that moment, all parameters are recorded in nominal operating conditions. This SoH is used as a reference, because it is considered as a healthy mode. Therefore, when these operating conditions deviate, the SoH of the PEMFC could be associated to a faulty mode. Obviously, the more important the deviation is, the more severe and damageable the fault on the fuel cell system will be. The fault considered here is a variation of the air stoichiometry ratio. This fault could be linked to a mysfunction of the air compressor and/or a fault. The acceptable ranges for the various operating parameters of the fuel cell are reported in Table 2.

For the specific case studied, the air stoichiometry can vary between 1.3 and 5. As previously mentioned in Table 1, the nominal value is 2. In order to create a high air stoichiometry fault, this value varies successively at higher air stoichiometry ratios than those recommended by the supplier. Fig. 3 gives the protocol of

Table 2
Range of variation of the parameters of functioning of the forty-cell stack.

Parameter	Range
Pressure	[100–250] kPa
Anode relative humidity	[0–100]%
Cathode relative humidity	[0–100]%
Hydrogen stoichiometry	[1.1–2]
Air stoichiometry	[1.3–5]
Stack temperature	[0–80] °C

the increasing of the air stoichiometry by taking different values (2–4 - 5–2), define by the different partners of the project.

Before changing this parameter, a stabilization phase at nominal operating conditions is necessary at the begining of the test. Then, the high air feeding is performed for two values (4 and 5) that represent two levels of severity of the air supply fault. It is necessary that initial and final conditions are similar so that the fault observed can be identified as reversible or not. In the same way, the beginning and the ending conditions will serve as samples for comparison between healthy and faulty modes. The evolution of the electrical, fluidic and thermal parameters of the fuel cell during the increase of the air stoichiometry are presented on Fig. 3. The given operating conditions are the following: temperature of 80 °C, gases humidity of 50%, both for the anode and the cathode side, the anode stoichiometry is 1.5 and the cathode stoichiometry is 2, 4, 5 and 2 again.

Table 3 presents the evolution of the cell and the stack voltages during the variation of the air stoichiometry for the three chosen values.

2.3. Impact of a high air stoichiometry fault occurrence

When the air stoichiometry increases, the membrane dries out [30] because the air flow is higher and evacuates the water produced by the electrochemical reaction. As explained in [31], the drying of the proton-conducting membrane implies a conductivity decrease which leads to higher ionic resistance and therefore to higher ohmic losses [32–34]. This results in a drop in cell potential [35,36] which is visible on Fig. 3, for an extra high air stoichiometry. Firstly, an increasing of the air stoichiometry is a benefit for the PEMFC. For a cathode stoichiometry of 4, instead of 2 (nominal value), the performances of the stack increase because more air and oxygen are available to react with the protons which pass through the membrane. However, if the stoichiometry continues to increase up to 5, the stack voltage decreases significantly. In

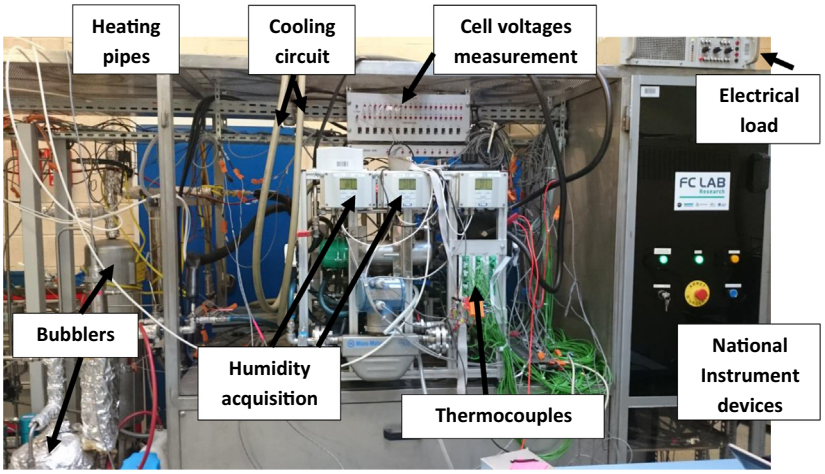

Fig. 2. 10 kW PEMFC test bench.

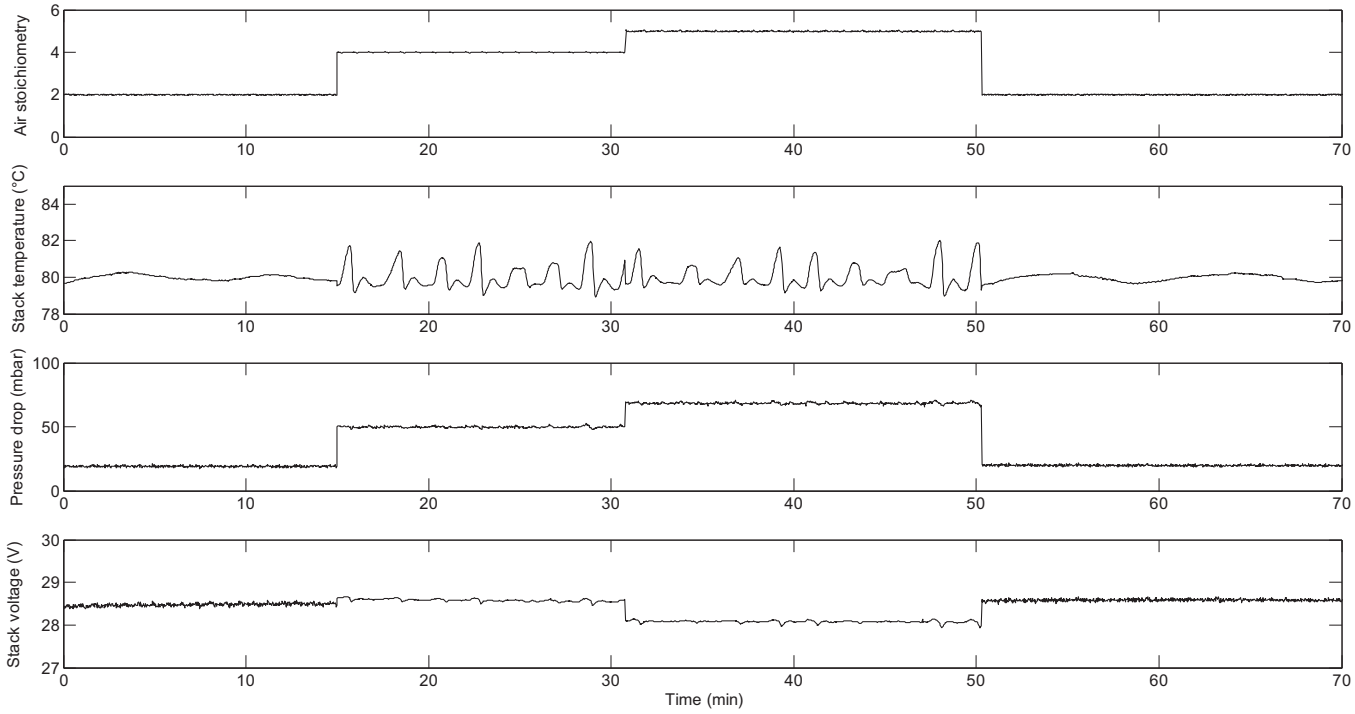

Fig. 3. Air stoichiometry, load current, stack temperature, pressure drop and stack voltage evolutions during an high air stoichiometry fault occurrence.

Table 3
Cell and stack voltages evolution according to three operating conditions.

HAS	Cell voltages			Stack voltage		
	Max	Min (V N°1)	Mean (V)	Max (V)	Min (V)	Mean (V)
2	0.73 V N°20	0.65	0.70	28.59	28.37	28.48
4	0.73 V N°28	0.66	0.72	28.67	28.46	28.58
5	0.72 V N°28	0.66	0.70	28.14	27.93	28.08
2	0.74 V N°28	0.65	0.72	28.67	28.48	28.58

the same time, the extra high air stoichiometry implies some stack temperature variations (±1—2 °C). Indeed, the nominal operating conditions (which are the most favorable to the smooth running of the fuel cell) are modified, so implying this fluctuating behavior of the stack temperature. Nevertheless, this temporary phenomena can be reversed by humidifying the membrane. The recovery time depends on the membrane thickness and the water diffusion coefficient [33–36]. In the case of drying condition over long time, the fault can cause serious and irreversible damage to the fuel cell membrane. Thus, a high air stoichiometry can be considered as a degraded functioning mode for the PEMFC. This fault could be considered as frequent on the fuel cell system [37]. The causes could be: a drift of the speed of the motor compressor unit, a mismanagement of the air flow reference, a delay on the air flow controller or a wrong estimation of the rotation speed of the motor. A high air stoichiometry influences directly the behavior of the pressure between the inlet and the outlet of the gas pipes. When the cathode stoichiometry increases, the outlet air pressure decreases (cf. Fig. 4). The control unit continues to regulate the inlet air pressure, but the outlet air pressure drops, that induces a higher difference of pressure between the inlet and the outlet on the air pipe. The air pressure is regulated at the inlet side. So the inlet air pressure is maintained at a constant value fixed in Table 1). When the air flow increases, the charge losses increase too, that is why the outlet air pressure has to be decreased in order to maintain the inlet air pressure constant. It can be observed that, the higher the stoichiometry ratio is, the more sensitive the behavior of the system is. This is expressed by the apparition of oscillations in the humidity and the temperature signals.

3. Diagnosis method

The fault diagnosis approach proposed in this paper belongs to the non model-based methods and more precisely to the signal-based methods. In a practical point of view, a WT is applied to an input signal (voltage or pressure) acquired on a PEMFC considered as in healthy or in faulty operating condition. The initial signal is split into high and low frequencies using the wavelet decomposition. The high frequency part is collected and analyzed through the assessment of the energy contained in the initial input signal. The energy content varies depending on the operating conditions [24–38]. For instance, the percentage of energy contained in a nominal operating condition signal is different from a faulty state signal (i.e. high air stoichiometry values). As a consequence, the relative wavelet energy contained in the input signal is used as an indicator of the SoH of the fuel cell system [39]. Moreover, the entropy of the high frequency part of the signal gives information about the state of the fuel cell. Thus, a combination of these informations (energy and entropy) seems to be very relevant for early diagnosis of a fuel cell system. Three different input signals are considered in this study, the air pressure drop between the inlet and the outlet of the stack, the stack voltage and the cell voltages. Firstly, the WT is described in Section 3.1 with some details about the wavelet decomposition and the frequency content and then a focus on the relative wavelet energy and the entropy of the input signal is presented.

3.1. Wavelet decomposition and reconstruction of a signal

The paper deals with discrete wavelet transform (DWT) which is a tool for the analysis of the output voltage signal with non-stationary and transient phenomena [40,41]. The DWT decomposes the signal (pressure or voltage in our work) in time

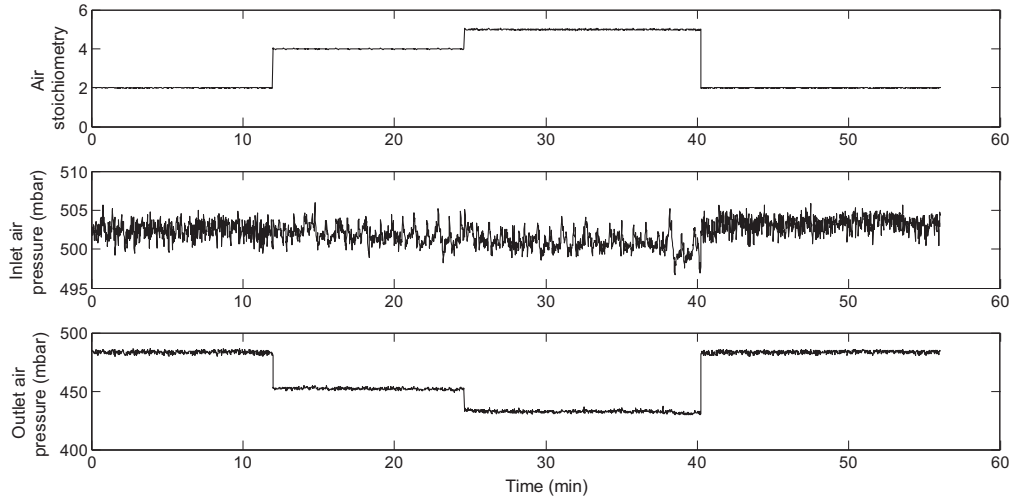

Fig. 4. Evolutions of the inlet and outlet air pressures when the cathode stoichiometry increases.

and frequency domains. The high frequency part of the initial signal $s(t)$ is expressed by details D_i and the low frequency part of the initial signal $s(t)$ is represented by approximations A_i [38]. In this specific case, the wavelet decomposition method acts like a filter of the signal by successively using a low-pass and a high-pass filter [17], as shown in Fig. 5. In this work, the orthogonal wavelet filter [42,43] *db*4 of the Daubechies family that is suitable for a wide range of applications [44] is selected as the wavelet function of the proposed approach [45]. This type of wavelet is widely used to solve various kind of problems thanks to its orthogonally, which is useful for localization and classification of disturbances [40,46,47].

As illustrated in Fig. 6, at each decomposition level only the approximation signal is filtered in a new approximation and a new detail.

The initial signal can be reconstructed thanks to the last approximation and the different details obtained. As an example, the reconstruction of the initial signal $s(t)$ is given by Eq. (1).

$$s(t) = cA_5 + cD_5 + cD_4 + cD_3 + cD_2 + cD_1 \quad (1)$$

In this work, the acquisition frequency is 1 Hz that implies some consecutive resulting frequency bands. The limits of the different frequencies bands are based on the sampling rate and on the level number n. For the detail D_1, the upper limit of the frequency band is half the sampling rate ($f_s.2^{-1}$), whereas the lower limit is ($f_s.2^{-2}$) [40]. In order to generalize, for each detail D_i, the upper limit frequency of the considered band crosses with the lower limit frequency of the detail D_{n-1}. The width of the frequency band of the detail D_i equals the half width of the frequency band of the detail D_{i-1}. The distribution of the frequencies is given in Fig. 7. The details D_i contains the information concerning the signal components with frequencies included within the interval $[2^{-(n+1)}f_s, 2^{-n}f_s]$ Hz. The

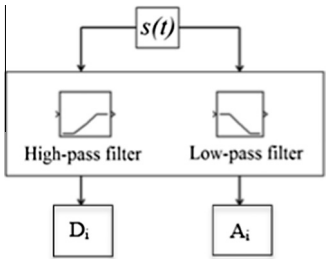

Fig. 5. Basic level of the wavelet transform filtering process.

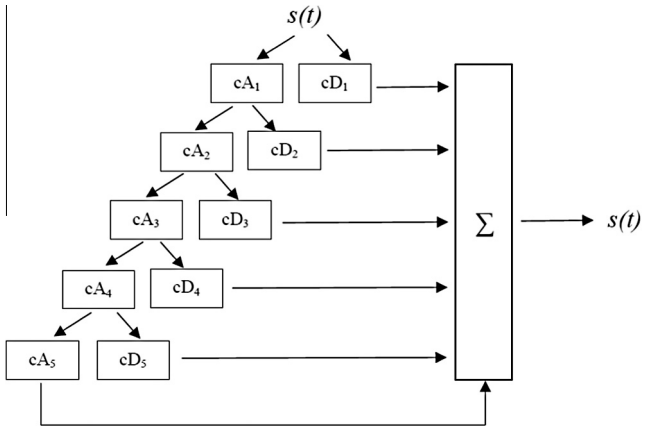

Fig. 6. Daubechies4 wavelet decomposition and reconstruction process with five levels.

approximations A_i contain the low-frequency components of the signal $s(t)$ that are included in the interval $[0, 2^{-(n+1)}f_s]$ [48]. The intervals here considered for all details D_i and the last approximation A_n are expressed in Table 4.

The most suitable decomposition level has to be selected depending on the nature of the signal and also on the faulty operating conditions. Considering the Section 2.3 and Fig. 8 [49], a high air stoichiometry implies a drying occurrence. Thus, the gas diffusion process is concerned and a membrane humidification is finally impacted by an increasing of the cathode stoichiometry. These faults cover the millisecond, second, minute and hour time domain.

A five-level decomposition allows investigating frequency domain comprised between 0 and 1 Hz (c.f. Table 4) that corresponds to a scale of one second to ten minutes for the fifth

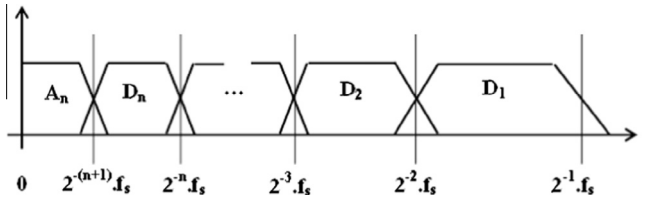

Fig. 7. Frequency bands corresponding to the DWT signal.

Table 4
Frequency bands obtained by decomposition in multi-levels.

Level number	Wavelet decomposition	Component type	Frequency band (Hz)
1	D_1	Detail	$[2^{-2}f_s, 2^{-1}f_s] = [0.250, 0.5]$ Hz
2	D_2	Detail	$[2^{-3}f_s, 2^{-2}f_s] = [0.125, 0.25]$ Hz
3	D_3	Detail	$[2^{-4}f_s, 2^{-3}f_s] = [0.063, 0.125]$ Hz
4	D_4	Detail	$[2^{-5}f_s, 2^{-4}f_s] = [0.031, 0.063]$ Hz
5	D_5	Detail	$[2^{-6}f_s, 2^{-5}f_s] = [0.016, 0.031]$ Hz
5	A_5	Approximation	$[0, 2^{-6}f_s] = [0, 0.016]$ Hz

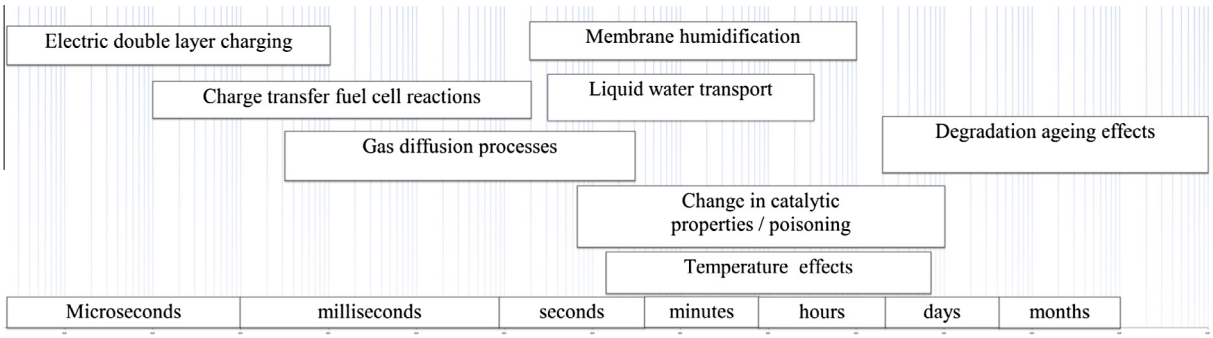

Fig. 8. Fuel cell stacks dynamic behavior [39].

level decomposition. In this way, Fig. 9 gives the approximation (A_5) and the details $(D_1 - D_5)$ by using the *db*4 wavelet for 5-level decomposition on the air pressure drop between the inlet and the outlet for the 40-cell PEMFC.

3.2. Relative wavelet energy (RWE)

To perform a signal wavelet decomposition, a wavelet family well adapted to the application has to be chosen as well as the level of the considered decomposition. These features are justified in the previous section. In this work, a focus is done on the energy contents of the signal $s(t)$ and especially on the energy contained in each detail $(D_1 - D_5)$. In the wavelet energy-based method, the wavelet energy is calculated for each component of the signal, therefore the energy distribution over the different frequency bands could be studied. This distribution can be treated as a representation of the information on the system process described by the studied signal [50]. For each detail D_i of the wavelet decomposition, which can be seen on the Fig. 9, the energy E_n^d is calculated thanks to Eq. (2).

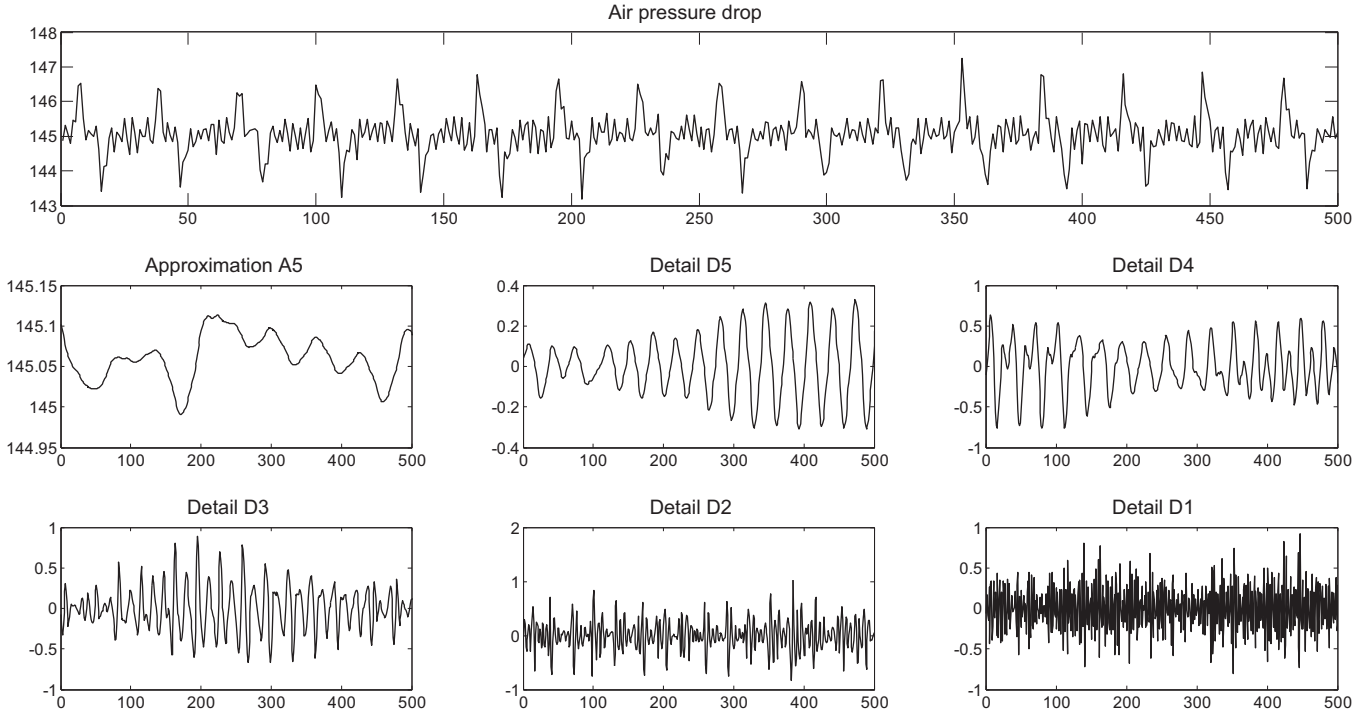

Fig. 9. Daubechies wavelet filtering of a cathode side pressure signal acquired on a 40-cell stack.

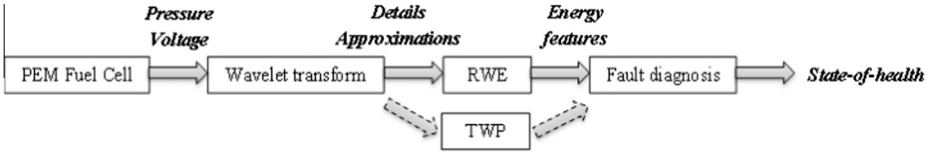

Fig. 10. Principle of the high air stoichiometry diagnosis process.

$$E_n^d = \sum_k \left| C_n^d(k) \right|^2 \tag{2}$$

where n is the level of decomposition.

The total energy of the signal is calculated by Eq. (3).

$$E_{tot}^d = \sum_n E_n^d \tag{3}$$

The RWE is the ratio between the energy of a detail and the total energy of the signal, obtained by summing the n detail energies of the signal:

$$\mathrm{RWE} = \frac{E_n^d}{E_t ot^d} \tag{4}$$

The vector that contains the percentages of energy and corresponds to the n details, measures the strength of fluctuation of the original signal at the relevant frequency band. The decomposition level choice is based on which kind of frequencies has to be observed by the user. The higher the decomposition level is, the more precise frequency scale is.

3.3. Total wavelet entropy (TWP)

The notion of entropy measures the amount of information contained in a signal. In other words, the entropy is a measure of the signal complexity. The total wavelet entropy (TWP) comes from Shannon entropy theory and gives a useful criterion for analyzing systems order/disorder by comparing probability distributions [51]. The TWP is defined as:

$$\mathrm{TWP} = -\sum_n p_n^d * \ln\left(p_n^d\right) \tag{5}$$

The smaller the TWP value is, the more regular and the less complex the signal is. A small value of TWP indicates that the energy distribution is in a high degree of regularity. For instance, the white noise is irregular random signal, its TWP is high, which means the signal has high complexity [52].

The degree of similarity of the energy distribution between two different signals can also be calculated by using the relative wavelet entropy (RWP) [38]. It is expressed as the summation of wavelet

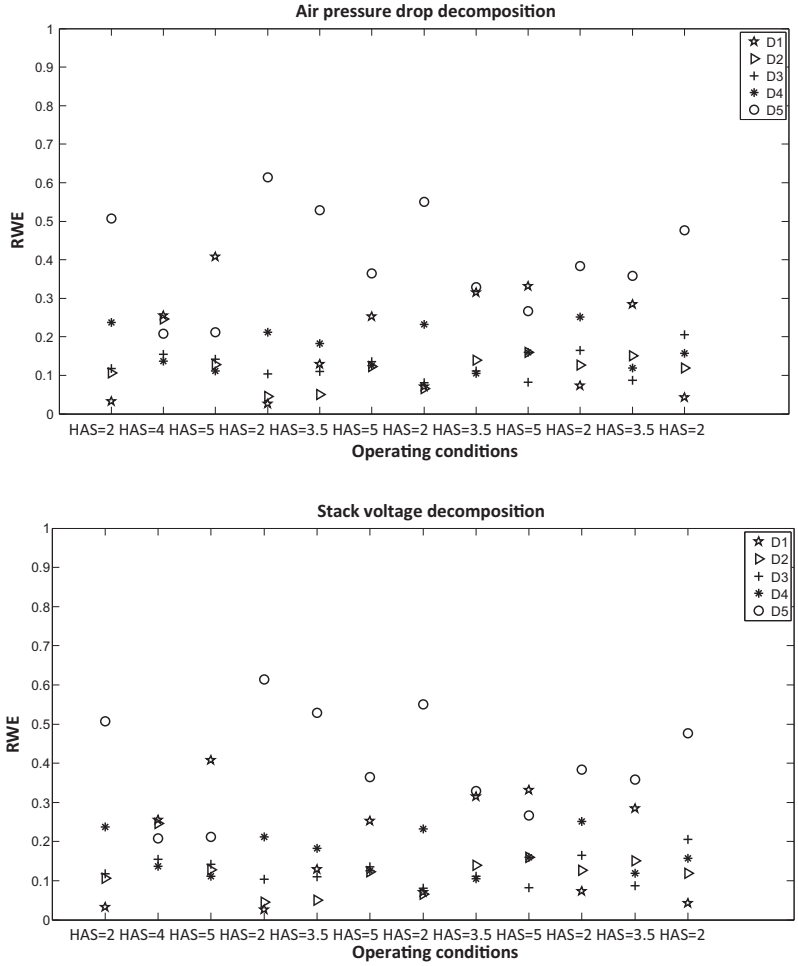

Fig. 11. RWE based on (a) the air pressure drop and (b) the stack voltage signals.

Table 5
Statistical analysis (minimum/maximum values, average and standard deviation) of the RWE contents of the details D_i for pressure drop ΔP and stack voltage U_{stack} signals, for different air stoichiometry ratios (HAS).

	HAS	Minimum					Maximum				
		D_1	D_2	D_3	D_4	D_5	D_1	D_2	D_3	D_4	D_5
ΔP	2	0.03	0.18	0.05	0.09	0.40	0.08	0.25	0.12	0.15	0.62
U_{stack}		0.03	0.05	0.09	0.18	0.38	0.08	0.12	0.15	0.25	0.62
ΔP	3.5	0.15	0.05	0.12	0.12	0.35	0.32	0.15	0.12	0.19	0.55
U_{stack}		0.15	0.05	0.10	0.10	0.32	0.32	0.15	0.12	0.18	0.52
ΔP	4	0.25	0.25	0.17	0.15	0.22	0.25	0.25	0.17	0.15	0.22
U_{stack}		0.26	0.25	0.15	0.13	0.20	0.26	0.25	0.15	0.13	0.20
ΔP	5	0.25	0.12	0.08	0.10	0.22	0.40	0.50	0.13	0.15	0.35
U_{stack}		0.25	0.12	0.08	0.10	0.22	0.40	0.17	0.15	0.15	0.35
$\times 10^{-3}$	HAS	Average					Standard deviation				
		D_1	D_2	D_3	D_4	D_5	D_1	D_2	D_3	D_4	D_5
ΔP	2	54	23	90	132	512	25	33	27	44	82
U_{stack}		57	92	132	216	502	25	31	44	25	92
ΔP	3.5	257	117	120	150	300	93	58	0	36	278
U_{stack}		257	117	113	131	397	33	58	12	42	108
ΔP	4	250	250	170	150	220	0	0	0	0	0
U_{stack}		260	250	150	130	200	0	0	0	0	0
ΔP	5	333	130	113	123	190	76	17	29	25	177
U_{stack}		323	137	120	123	283	75	29	36	25	65

coefficients within a selected frequency range over the time [53], defined as:

$$S_{WT}(p \mid q) = \sum_n p_n^d * ln\left(\frac{p_n^d}{q_n^d}\right) \quad (6)$$

where q_n^d denotes the relative energy of the nth level detail sub-signal of a reference signal.

Fig. 10 allows summing up, the different steps required for the fault diagnosis of the PEM fuel cell stack. A signal (pressure or voltage) is firstly processed by WT analysis to decompose it into various details and approximations parts, depending on a multi-scale decomposition. Then the RWE is calculated thanks to Eqs. (2)–(4) in order to evaluate the energy content of the initial signal $s(t)$ in three different faulty conditions (HAS = 3.5, HAS = 4, HAS = 5) and also in the nominal operating conditions HAS = 2). Depending on RWE value, a deviation of the nominal operating conditions can be isolated and the SoH of the fuel cell system can be estimated. In addition, the TWP should help as an additional estimation.

4. Results

In this section, some results based on the method described on Fig. 10 and applied to the 40-cell stack, are presented. Three different signals are used to perform the fault diagnosis, namely the pressure drop between the inlet and the outlet of the cathode side of the PEMFC, the stack voltage and the different single cell

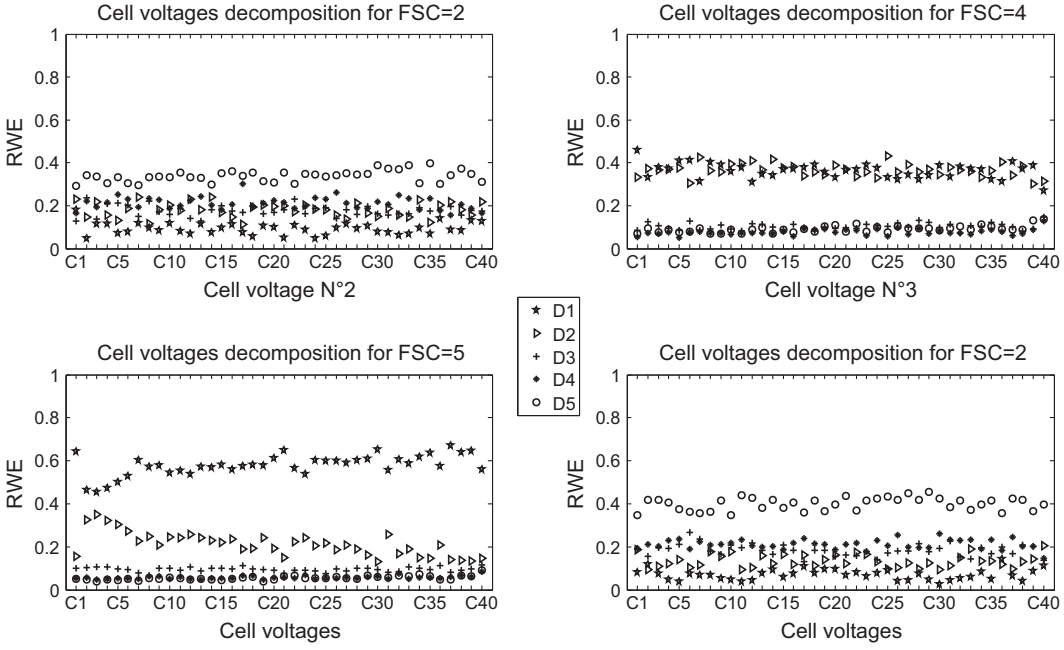

Fig. 12. RWE of the forty cell voltages.

Table 6
Energy content of details D_i according to air stoichiometry (HAS) evolution.

	HAS = 2					HAS = 4				
	D_1	D_2	D_3	D_4	D_5	D_1	D_2	D_3	D_4	D_5
Minimum	0.04	0.12	0.12	0.15	0.28	0.28	0.28	0.05	0.04	0.05
Maximum	0.18	0.25	0.22	0.30	0.38	0.45	0.42	0.13	0.12	0.13
Average	0.10	0.18	0.18	0.21	0.33	0.35	0.35	0.10	0.07	0.09
Standard deviation	0.03	0.03	0.03	0.03	0.03	0.04	0.03	0.02	0.02	0.02
	HAS = 5					HAS = 2				
Minimum	0.45	0.13	0.05	0.04	0.03	0.01	0.08	0.13	0.15	0.35
Maximum	0.64	0.35	0.12	0.09	0.10	0.15	0.20	0.26	0.26	0.45
Average	0.57	0.22	0.10	0.06	0.06	0.06	0.13	0.21	0.21	0.40
Standard deviation	0.04	0.05	0.02	0.01	0.01	0.03	0.03	0.02	0.02	0.03

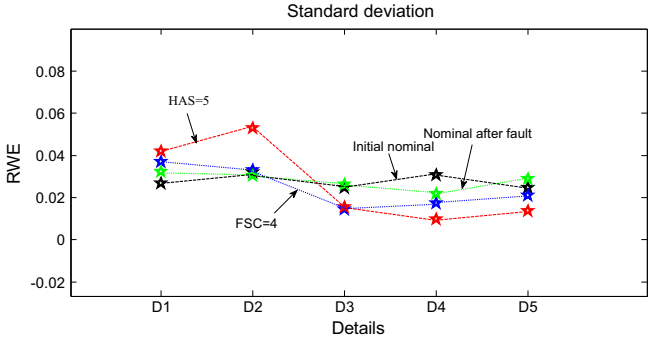

Fig. 13. Standard deviation of the RWE contained in details D_i according to cathode stoichiometry (HAS) for cell voltage input signal.

voltages. For each study, the repartition of energy contained per detail, E_n^d, is expressed versus the operating conditions. In order to prove the reproducibility of the method, some tests are made at different days, after a complete shut down of the fuel cell stack. Twelve operating conditions are given which represent four different days of test. They all start with nominal operating conditions (HAS = 2) and then an increase of HAS value up to 5 is considered, finally the nominal operating conditions are applied another time (c.f. Fig. 11). In other words: the first day, the air stoichiometry is increased twice because HAS equals 2 (nominal) then 4 and finally 5. The second day, HAS equals to 2 (nominal) then 3.5 and finally 5, and so on for the remaining conditions. The RWE for the five detail signals are represented by a different symbol depending on the operating conditions and according to the initial signal used for the diagnosis. Considering the last detail D_5, the higher the air stoichiometry is, the less important the energy content of the detail is. Conversely for the detail D_1, the higher the air stoichiometry is, the more important the energy content of the detail is. That is the case for both RWE calculated based on the pressure signal and also for the stack voltage signal.

Table 5 presents the statistical analyses of detail components ($D_1 - D_5$) depending on the evolution of the cathode stoichiometry. The case (HAS = 2) includes the five tests performed among the twelve proposed on Fig. 11. The case (HAS = 3.5) gathers the three tests at the considered operating mode, and so on. The case (HAS = 4) is tested just once, it can not be considered here. The aim is to quantify the reproducibility of the method. For each operating condition, the top value corresponds to the pressure signal and the second one to the stack voltage signal. The minimum, the maximum, the average and the standard deviation of the RWE of each detail are thus calculated. The results reported on Table 5 confirm the initial observation concerning the behaviors of the details D_1 and D_5. The global standard deviation illustrates a good reproducibility of the method.

Fig. 12 illustrates the same methodology applied on the individual cell voltages. The repartition of the RWE for the 5 details all along the cells is presented for two increasing levels of the air

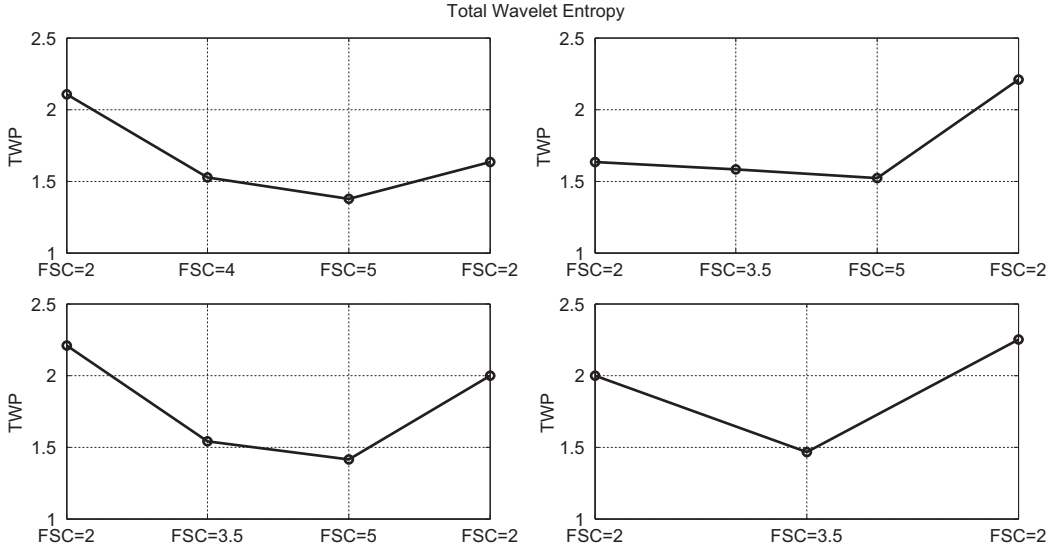

Fig. 14. TWP of the signal voltage input signal according to various operating modes.

stoichiometry. A change of the energy contained in each detail can be easily observed. This evolution is visible depending on the operating conditions tested, independently of the cell number. For the nominal mode, the detail which contains most energy is D_5 followed by D_2, D_3, D_4 and D_1 respectively. When the air stoichiometry increases (HAS = 4), the details are split into two groups, one on the top with details D_5 et D_2 and at the bottom the others. If the air stoichiometry keeps increasing, the detail D_1 is made distinguishable from the others. Thus, a huge repartition of the energy is observed. It is observed that the most energetic detail becomes the less energetic one.

During normal mode, the detail D_1 is constituted of 40% of total energy, conversely at high air stoichiometry (faulty mode), it is D_5 who gets about 60% of the total energy. After creating a reversible fault on the fuel cell system, the same behavior as the initial normal mode is observed. That confirms the reversible impact of the stoichiometry fault. By studying the percentage of energy contained in the two extreme details D_1 and D_5 and their distributions with regard to the others, an efficient fault diagnosis can be highlighted.

Table 6 shows the state and the energy content of each detail D_i according to the of the air stoichiometry (HAS). Once again, the behavior of both details D_1 and D_5 is the same. When the cathode stoichiometry increases, the energy content of the detail D_1 increases and the energy content of the detail D_5 decreases. Fig. 13 shows the standard deviation of the RWE for each detail D_i according to cathode stoichiometry.

On the other part, the RWP proposed a trend to diagnose a deviation from the nominal and healthy operating condition. Fig. 14 shows that the higher the air stoichiometry is, the lower the TWP is. That means the energy distribution is in a high degree of irregularity and complexity. As said in Section 3.3, the TWP indicator should confirm the fault diagnosis and ensure the true estimation of the fuel cell SoH.

5. Conclusion

In this paper, a novel signal-based fault diagnosis approach is described. Various kind of signals are recorded from a 40-cell stack in different operating conditions (healthy and abnormal modes). In this paper, only one type of fault (high air stoichiometry) has been used to verify the usability of the fault diagnosis method. The experimental conditions tested are directly linked to the air stoichiometry ratio. Based on properly defined protocols, the same faults (HAS = 3.5, HAS = 5) are reproduced several times, in order to collect a large database. It is very important to validate the generalization ability and the reproducibility of the proposed diagnosis approach. A high air stoichiometry fault is chosen and studied to apply relative wavelet energy, RWE-based method for fault diagnosis. Three different signals are selected and monitored directly from a PEMFC: the stack voltage signal, the cell voltages signals and the air pressure drop. The voltages signals can be collected without adding further sensors on the system. That is a huge advantage regarding the actual implementation. Some promising results are obtained by studying the energy contents in the details of the WT. When a deviation from the nominal working conditions of the fuel cell system appears, the most energetic detail changes, and the distribution of the detail energy values as well. The deviation from the nominal operating conditions is also ensured by the TWP-based approach to verify the SoH estimation and validate the previous fault diagnostics. Thanks to this methodology based on mathematical equations, a robust diagnostics can be obtained for a high air stoichiometry ratio. Future approaches should focus on the following aspects: (i) a wider study of the wavelet families to use; (ii) a wider comparison between the different results coming from the choice of the wavelet; (iii) a wider study of the faults tested on the 40-cell stack; (iv) a general fault diagnosis results about combinations of faults and wavelet choices.

Acknowledgements

The authors acknowledge French ANR projects DIAPASON1 & DIAPASON2 and also the Labex ACTION, ANR-11-LABX-01-01, for financially supporting these works and offering the possibility of using their data.

References

[1] Multi-year research, development and demonstration plan, hydrogen, fuel cells and infrastructure technologies program. Planned program activities for 2005–2015; March 2007. p. 332.
[2] Marcinkoski J, Kopasz JP, Benjamin TG. Progress in the US DOE fuel cell subprogram efforts in polymer electrolyte fuel cells. Int J Hydrogen Energy 2008;33:3894–902.
[3] Wang Y, Chen KS, Mishler J, Cho SC, Adroher XC. A review of polymer electrolyte membrane fuel cells: technology, applications, and needs on fundamental research. Appl Energy 2011;88:981–1007.
[4] Multi-year research, development and demonstration plan, technical plan-fuel cells. U.S. Department of Energy; 2012. p. 3.4-10–3.4-11. <http://energy.gov/sites/prod/files/2014/03/f12/fuel_cells.pdf>.
[5] Carlson EJ, Kopf P, Sinha J, Sriramulu S,Yang Y. Cost analysis of PEM fuel cell systems for transportation. National Renewable Energy Laboratory subcontract report 2005. US Department of Commerce, National Technical Information Service, Springfield, VA; 2005.
[6] Pei P, Chen H. Main factors affecting the lifetime of proton exchange membrane fuel cells in vehicle applications: a review. Appl Energy 2014;125:60–75.
[7] Petrone R, Zheng Z, Hissel D, Pra MC, Pianese C, Sorrentino M, et al. A review on model-based diagnosis methodologies for PEMFCs. Int J Hydrogen Energy 2013:7077–93.
[8] Zheng Z, Petrone R, Pra MC, Hissel D, Becherif M, Pianese C, et al. A review on non-model based diagnosis methodologies for PEM fuel cell stacks and systems. Int J Hydrogen Energy 2013:1–13.
[9] Meidanshahi V, Karimi G. Dynamic modeling, optimization and control of power density in a PEM fuel cell. Appl Energy 2012;93:98–105.
[10] Yan WM, Wang XD, Lee DJ, Zhang XX, Guo YF, Su A. Experimental study of commercial size proton exchange membrane fuel cell performance. Appl Energy 2011;88:392–6.
[11] Hosseinzadeh E, Rokni M, Rabbani A, Mortensen HH. Thermal and water management of low temperature proton exchange membrane fuel cell in fork-lift truck power system. Appl Energy 2013;104:434–44.
[12] Bonvini M, Sohn MD, Granderson J, Wetter M, Piette MA. Robust on-line fault detection diagnosis for HVAC components based on nonlinear state estimation techniques. Appl Energy 2014;124:156–66.
[13] Rabbani A, Rokni M. Effect of nitrogen crossover on purging strategy in PEM fuel cell systems. Appl Energy 2013;111:1061–70.
[14] Da Fonseca R, Bideaux E, Gerard M, Jeanneret B, Desbois-Renaudin M, Sari A. Control of PEMFC system air group using differential flatness approach: validation by a dynamic fuel cell system model. Appl Energy 2014;113:219–29.
[15] Gerard M, Poirot-Crouvezier JP, Hissel D, Pera MC. Oxygen starvation analysis during air feeding faults in PEMFC. Int J Hydrogen Energy 2010;35:12295–307.
[16] Iosevich A, Liflyand E. Basic properties of the fourier transform, decay of the Fourier transform. Anal Geomet Aspects 2014:11–6.
[17] Mallat S. A wavelet tour of signal processing. Third edition: the sparse way. Academic Press; 2008 [p. 832, ISBN: 978-0-12-374370-1].
[18] Bouzida A, Touhami O, Ibtiouen R, Belouchrani A, Fadel M, Rezzoug A. Fault diagnosis in industrial induction machines through discrete wavelet transform. IEEE Trans Ind Electron 2011;58(9):4385–95.
[19] Giaouris D, Finch JW, Ferreira OC, Kennel RM, Elmurr GM. Wavelet denoising for electric drives. IEEE Trans Ind Electron 2008;55(2):543–50.
[20] Liu H, Tian HQ, Pan DF, Li YF. Forecasting models for wind speed using wavelet, wavelet packet, time series and artificial neural networks. Appl Energy 2013;107:191–208.
[21] Wang JZ, Wang Y, Jiang P. The study and application of a novel hybrid forecasting model – a case study of wind speed forecasting in China. Appl Energy 2015;143:472–88.
[22] Du Z, Jin X, Yang Y. Fault diagnosis for temperature, flow rate and pressure sensors in VAV systems using wavelet neural network. Appl Energy 2009;86:1624–31.
[23] Ibrahim M, Jemei S, Hissel D, Wimmer G. On-board energy management for a hybrid vehicle: wavelet based approach. Int Scient Conf Hybrid Electr Vehic (RHEVE) 2011:1–8.
[24] Yousfi Steiner N, Wang K, Péra MC, Hissel D. Localisation d un ou plusieurs défauts dans un ensemble électrochimique, brevet d invention; demande prioritaire: FR 12 62319. Extension de la protection N: PCT/FR2013/053163 dépôt; Novembre, 2012.

[25] Yousfi Steiner N, Hissel D, Mooteguy P, Candusso D. Non intrusive diagnosis of polymer electrolyte fuel cells by wavelet packet transform. Int J Hydrogen Energy 2011;36:740–6.
[26] Projet DIAPASON2, 2011–2014. <http://www.agence-nationale-recherche.fr/?Projet=ANR-10-HPAC-0002>.
[27] Zhongliang L, Outbib R, Giurgea S, Hissel D, Li Y. Fault detection and isolation for polymer electrolyte membrane fuel cell systems by analyzing cell voltage generated space. Appl Energy 2015;148:260–72. http://dx.doi.org/10.1016/j.apenergy.2015.03.076.
[28] Benouioua D, Candusso D, Harel F, Oukhellou L. PEMFC stack voltage singularity measurement and fault classification. Int J Hydrogen Energy 2014;39(36):21631–7. http://dx.doi.org/10.1016/j.ijhydene.2014.09.117.
[29] Pahon E, Oukhellou L, Harel F, Samir J, Hissel D. Fault diagnosis and identification of proton exchange membrane fuel cell system using electrochemical impedance spectroscopy classification. In: 11th International conference on modeling and simulation of electric machines, converters and systems, ElectrIMACS 2014. Valence, Spain; 2015. p. 646–51.
[30] Pozio A, Cemmi A, Mura F, Masci A, Serra E, Silva RF. Long-term durability study of perfluoropolymer membranes in low humidification conditions. J Solid State Electrochem 2011;15:1209–16.
[31] Schmittinger W, Vahidi A. A review of the main parameters influencing long-term performance and durability of PEM fuel cells. J Power sources 2008;180:1–14.
[32] Hinds G. NPL report DEPC-MPE 002; 2004. p. 25–42.
[33] Le Canut J-M, Abouatallah RM, Harrington DA. Detection of membrane drying, fuel cell flooding and anode catalyst poisoning on PEMFC stacks by electrochemical impedance spectroscopy. J Electrochem Soc 2006;153:A857–64.
[34] Sone Y, Ekdunge P, Simonsson D. Proton conductivity of Nafion 117 as measured by a four electrode AC impedance method. J Electrochem Soc 1996;143:1254–9.
[35] Nguyen TV, White RE. A water and heat management model for proton exchange membrane fuel cells. J Electrochem Soc 1993;140:2178–86.
[36] Wang Y, Wang CY. Dynamics of polymer electrolyte fuel cells undergoing load changes. Electrochim Acta 2006;51:3924–33.
[37] Qu S, Li X, Hou M, Shao Z, Yi B. The effect of air stoichiometry change on the dynamic behavior of a proton exchange membrane fuel cell. J Power Sources 2008;185:302–10.
[38] Wang K. Algorithmes et Méthodes pour le diagnostic ex-situ et in-situ de systmes piles combustible haute température de type oxyde solide. PhD thesis, University of Franche-Comte; 2012. p. 168.
[39] Pahon E, Yousfi-Steiner N, Jemei S, Mooteguy P, Hissel D. A signal-based method for a proton exchange membrane fuel cell fault diagnosis. In: 6th International conference on fundamentals and developments of fuel cells, FDFC'2015. Toulouse, France; 2015. p. 8.
[40] Goharrizi AY, Sepehri N. A wavelet-based approach to internal seal damage diagnosis in hydraulic actuators. IEEE Trans Ind Electron 2010;57(5):1755–63.
[41] Guasp MR, Daviu JAA, Sanchen MP, Panadero RP, Cruz JP. A general approach for the transient detection of slip-dependent fault components based ont he discrete wavelet transform. IEEE Trans Ind Electron 2008;55(12):4167–80.
[42] Daubechies I. Ten lectures on wavelets. SIAM; 1992 [p. 350, ISBN: 978-0-89871-274-2].
[43] Daubechies I. The wavelet transform, time-frequency localization and signal analysis. IEEE Trans Inform Theory 1990;IT-36:961–1005.
[44] Barelli L, Barluzzi E, Bidini G, Bonucci F. Cylinders diagnosis system of a 1MW internal combustion engine through vibrational signal processing using DWT technique. Appl Energy 2012;92:44–50.
[45] Kim J, Chun CY, Cho BH. Discrimination and state-of-health diagnosis based on the discrete wavelet transform for a polymer electrolyte membrane fuel cell. In: Twenty-eighth annual IEEE 2013, applied power electronics conference and exposition (APEC); 2013. p. 3351–7.
[46] Sen C, Usama Y, Carciumaru T, Lu X, Kar NN. Design of a novel wavelet based transient detection unit for in-vehicle fault determination and hybrid energy storage system. IEEE Trans Smart Grid 2012;1:422–33 [3].
[47] Hsia CH, Guo JM. Efficient modified directional lifting-based discrete wavelet transform for moving object detection. Signal Process 2014;96:138–52.
[48] Yan R, Gao RX, Chen X. Wavelets for fault diagnosis of rotary machines: a review with applications. Signal Process 2014;96:1–15.
[49] Wang H, Yuan XZ, Li H. PEM fuel cell diagnostic tools. CRC Press; 2011 [p. 578, ISBN 9781439839195].
[50] Peng ZK, Chu FL. Application of the wavelet transform in machine condition monitoring and fault diagnostics: a review with bibliography. Mech Syst Signal Process 2014;18:199–221.
[51] Yordanova J, Kolev V, Rosso OA, Schrmann M, Sakowitz OW, Zgren M, et al. Wavelet entropy analysis of event-related potentials indicates modality-independent theta dominance. J Neurosci Methods 2002;117:99–109.
[52] Zheng-You HE, Xiaoqing C, Guoming L. Wavelet entropy measure definition and its application for transmission line fault detection and identification. Int Conf Power Syst Technol 2006:1–6.
[53] Emre Cek M, Ozgoren M, Acar Savaci F. Continuous time wavelet entropy of auditory evoked potentials. Comput Biol Med 2010;40:90–6.